

## Growth and characterization of $^{28}\text{Si}_n/^{30}\text{Si}_n$ isotope superlattices

T. Kojima, R. Nebashi, and K. M. Itoh<sup>a)</sup>

*Department of Applied Physics and CREST-JST, Keio University, Yokohama 223-8522, Japan*

Y. Shiraki

*Department of Applied Physics, The University of Tokyo, Tokyo 113-8656, Japan*

(Received 20 May 2003; accepted 6 August 2003)

We present silicon isotope superlattices: Si structures in which alternating layers are predominantly composed of the stable isotopes  $^{28}\text{Si}$  and  $^{30}\text{Si}$ . Using solid-source molecular beam epitaxy, the thickness of each isotope layer has been precisely controlled to produce isotope superlattices denoted  $^{28}\text{Si}_n/^{30}\text{Si}_n$ , where  $n$  is the number of atomic monolayers, each one 0.136 nm thick. We have produced and studied  $^{28}\text{Si}_8/^{30}\text{Si}_8$ ,  $^{28}\text{Si}_{12}/^{30}\text{Si}_{12}$ , and  $^{28}\text{Si}_{24}/^{30}\text{Si}_{24}$ , whose structures have been confirmed by secondary ion mass spectrometry. Further confirmation was provided by Raman spectroscopy, which showed the confinement of phonons within specific isotope layers ( $^{28}\text{Si}$  or  $^{30}\text{Si}$  layers) due to the mass periodicity created by isotope layering. © 2003 American Institute of Physics. [DOI: 10.1063/1.1613365]

In the era of atomic-scale materials physics, it is natural to expect that mass numbers (isotopes) and nuclear spin states (also isotopes) will play important roles even when the material is composed of a single element. For example, naturally available silicon ( $^{\text{nat}}\text{Si}$ ) is always composed of three stable isotopes in fixed proportions:  $^{28}\text{Si}$  (92.2 at. %),  $^{29}\text{Si}$  (4.7 at. %), and  $^{30}\text{Si}$  (3.1 at. %). The mass difference of  $\sim 7\%$  between  $^{28}\text{Si}$  and  $^{30}\text{Si}$  isotopes may be an important determinant of the properties of silicon nanostructures that were widely studied recently.<sup>1</sup> Improvement of electronic transport and/or optical properties via manipulation of the vibrational (phonon) modes based on atomic scale isotope engineering may be possible because of the strong influence of electron-phonon interactions on a variety of electronic and optical properties. It is also possible to control the nuclear spin properties through manipulation of Si isotopes since  $^{28}\text{Si}$  and  $^{30}\text{Si}$  isotopes have no nuclear spin moment while  $^{29}\text{Si}$  has a moment of  $I = 1/2$ . It has been shown that nuclear spin control is important for some of the most realistic schemes for the development of quantum computers based on silicon,<sup>2,3</sup> and that the ability to stack Si isotopes layer-by-layer is crucial for realization of them.

Experimental investigation of isotope effects in semiconductors was pioneered at Bell Labs in the 1950's.<sup>4-6</sup> Molecular beam epitaxy (MBE) of isotopically controlled germanium has enabled studies of low dimensional phonons in isotope superlattices<sup>7-9</sup> and quantum dots.<sup>10</sup> Haller provides an excellent summary of isotopically engineered semiconductors up to 1994.<sup>11</sup> More recently, a variety of "new" isotope effects on optical properties of silicon<sup>12-15</sup> has been discovered thanks to the recent successful growth of high quality isotopically enriched  $^{28}\text{Si}$  (Refs. 16-18),  $^{29}\text{Si}$  (Ref. 19), and  $^{30}\text{Si}$  (Ref. 19) bulk single crystals. Thick  $^{28}\text{Si}$  films grown on  $^{\text{nat}}\text{Si}$  substrates have contributed greatly to self-diffusion studies which provide important parameters for the development of future Si IC process.<sup>20-22</sup> However, isotope

effects in Si nanostructures have yet to be investigated because Si isotope superlattices and quantum dots have never been available, unlike the case for germanium.<sup>7-10</sup>

In this work we have grown three kinds of silicon isotope superlattices ( $^{28}\text{Si}_n/^{30}\text{Si}_n$  with  $n = 8, 12,$  and  $24$ ) using the solid-source MBE technique (Fig. 1). Here  $n$  denotes the thickness of each isotope layer in atomic monolayers, each 0.136 nm thick. The periodicities, i.e., the number of  $^{28}\text{Si}/^{30}\text{Si}$  pair layers stacked vertically, are 80, 50, and 30 for  $n = 8, 12,$  and  $24$  samples, respectively. The resulting total thicknesses of the superlattices are 160–200 nm. The source for the  $^{28}\text{Si}$  layer is actually  $^{\text{nat}}\text{Si}$  which is composed of 92.2%  $^{28}\text{Si}$ . The source for the  $^{30}\text{Si}$  layer is a single Si crystal isotopically enriched to  $^{30}\text{Si} = 98.74\%$  as reported in Ref. 19. In our MBE process,  $^{28}\text{Si}$  and  $^{30}\text{Si}$  solid sources are melted in individual effusion cells equipped with crucibles made of high purity tantalum. The crucible temperature is maintained at 1400 °C for a growth rate of  $\sim 0.01$  nm/s. The cell typically introduces  $10^{16}$ – $10^{17}$   $\text{cm}^{-3}$  aluminum impurities in the grown layer, most likely due to residual aluminum in the tantalum. The Si substrates we employ are (100) Cz-Si wafers (resistivity  $> 10 \Omega \text{ cm}$ ), and they are preannealed at

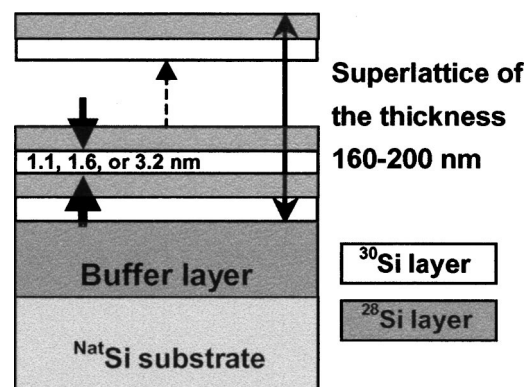


FIG. 1. Schematics of Si isotope superlattices grown in this work. Thicknesses of each isotope layer are 1.1, 1.6, and 3.2 nm for  $^{28}\text{Si}_8/^{30}\text{Si}_8$ ,  $^{28}\text{Si}_{12}/^{30}\text{Si}_{12}$ , and  $^{28}\text{Si}_{24}/^{30}\text{Si}_{24}$  samples, respectively.

<sup>a)</sup>Electronic mail: kitoh@appi.keio.ac.jp

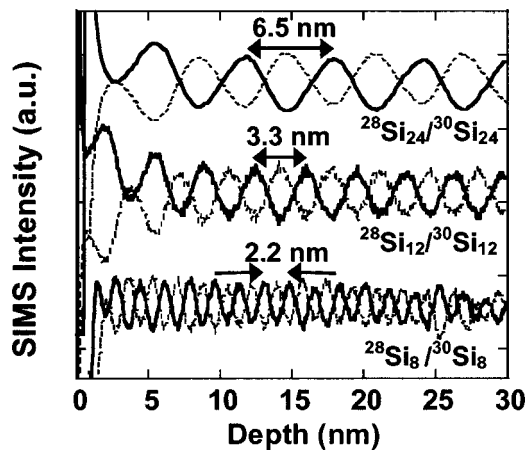


FIG. 2. Depth profile of  $^{28}\text{Si}$  (solid curves) and  $^{30}\text{Si}$  (dashed curves) in the  $^{28}\text{Si}_8/^{30}\text{Si}_8$ ,  $^{28}\text{Si}_{12}/^{30}\text{Si}_{12}$ , and  $^{28}\text{Si}_{24}/^{30}\text{Si}_{24}$  samples revealed by secondary ion mass spectroscopy (SIMS). Periods of oscillations 2.2, 3.3, and 6.5 nm corresponds exactly to those expected for  $n=8$ , 12, and 24 superlattices, respectively.

850 °C followed by buffer layer growth at 750 °C and superlattice growth at 650 °C. The base pressure of the vacuum is  $5 \times 10^{-10}$  Torr and the pressure during growth is  $\sim 10^{-9}$  Torr. The depth profile of the  $^{28}\text{Si}$  and  $^{30}\text{Si}$  isotope concentrations is determined with the ATOMICA 6500 secondary ion mass spectrometer (SIMS). Raman spectra of the three superlattices are recorded in backscattering geometry at  $T \sim 4$  K using the  $\text{Ar}^+$  514 nm line.

Figure 2 shows the depth profile of  $^{28}\text{Si}$  and  $^{30}\text{Si}$  isotopes measured by SIMS in the  $^{28}\text{Si}_8/^{30}\text{Si}_8$ ,  $^{28}\text{Si}_{12}/^{30}\text{Si}_{12}$ , and  $^{28}\text{Si}_{24}/^{30}\text{Si}_{24}$  samples. As expected, out-of-phase oscillations of the  $^{28}\text{Si}$  and  $^{30}\text{Si}$  isotopes are observed clearly as a function of depth, confirming that we have successfully fabricated the superlattices. The mass periodicities of 2.2, 3.3, and 6.5 nm expected for the  $n=8$ , 12, and 24 samples, respectively, are observed clearly, though this fluctuates somewhat in the  $n=8$  samples. This fluctuation specific to the  $n=8$  sample is due to the fact that we were running out of both  $^{28}\text{Si}$  and  $^{30}\text{Si}$  sources during this particular growth, since it was the last sample we fabricated of the three. The sinusoidal character of the signal variations in Fig. 2 might appear to indicate gradual rather than abrupt boundaries between the isotope layers, since abrupt boundaries might be expected to produce a square waveform. However, this smearing out is an unavoidable artifact due to mixing of  $^{28}\text{Si}$  and  $^{30}\text{Si}$  isotopes caused by sputtering involved in SIMS, and the actual interface is abrupt with very small intermixing (less than a few layers) as we will confirm in the following Raman analysis.

Raman spectroscopy has been performed in order to show that it is indeed possible to manipulate phonon properties through nanoscale thickness control of the isotopic layers, and that the  $^{28}\text{Si}/^{30}\text{Si}$  interfaces in our isotope superlattices are abrupt. The  $E$  vs  $k$  dispersion of phonons in the superlattice is zone-folded due to the new periodicity,  $n a$ , introduced by the  $(^{28}\text{Si})_n-(^{30}\text{Si})_n$  unit where  $a$  is the periodicity of the bulk Si. Because Raman spectroscopy, to the first order, probes phonons situated at  $k \sim 0$  in the dispersion relation, while only one longitudinal optical (LO) phonon peak is observed with bulk Si, multiple LO phonon peaks should

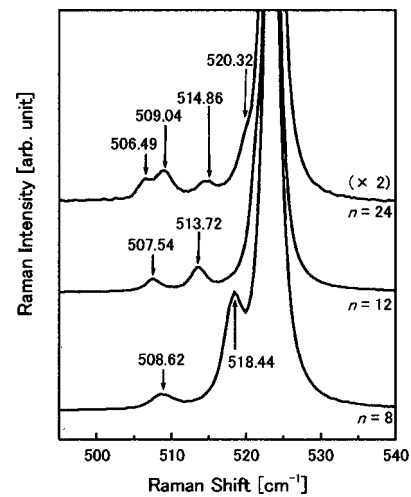


FIG. 3. Raman spectra of the  $^{28}\text{Si}_n/^{30}\text{Si}_n$  samples with  $n=8$ , 12, and 24.

appear for isotope superlattices due to the zone folding or phonon localization. Figure 3 shows the Raman spectra of the superlattices. As expected, many peaks are observed on the shoulders of the large  $^{\text{nat}}\text{Si}$  substrate LO peak around  $523.5 \text{ cm}^{-1}$ . The wave numbers of the identified peaks are indicated in the figure for comparison with theoretical predictions. In parallel, phonon frequencies expected for each superlattice have been calculated theoretically, using the planar bond-charge model for Si.<sup>23</sup> Details of our calculations including notations for different vibrational modes [ $\text{LO}_1(^{28}\text{Si})$ ,  $\text{LO}_1(^{30}\text{Si})$ , etc.] are same as the case of the Ge isotope superlattices described in Refs. 7 and 24. Figure 4 shows the Raman peak positions for our  $^{28}\text{Si}_n/^{30}\text{Si}_n$  superlattices as a function of the layer thickness  $n$ . Solid curves are the predictions of theory while triangles represent the experimentally observed peaks shown in Fig. 3. The actual isotopic composition of  $^{28}\text{Si}$ ,  $^{29}\text{Si}$ , and  $^{30}\text{Si}$  isotopes in each  $^{28}\text{Si}$  and  $^{30}\text{Si}$  layer is properly accounted for in our theoretical calculations. Similar to the case in Ref. 7 for Ge isotope superlattices, the theoretical peak positions are shifted rigidly to lower frequencies by  $\sim 5 \text{ cm}^{-1}$  in order to account for a small deficiency of the fits for bulk  $\mathbf{k}=0$  phonons and the effect of isotope disorder.<sup>25</sup> Theoretical curves are not smooth due to anticrossings. In general, the agreement between the experimental and theoretical results is excellent

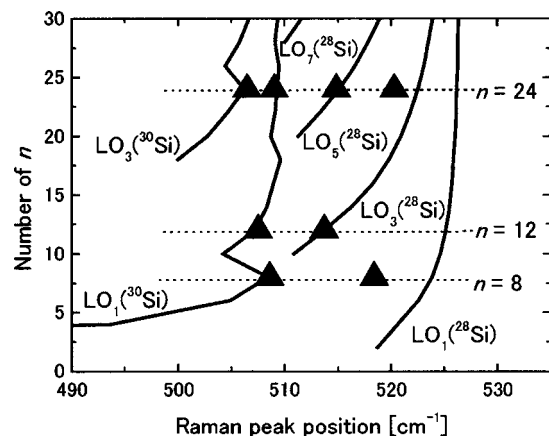


FIG. 4. Direct comparison of theory (solid curves) and experimentally found peak positions ( $\blacktriangle$ ) as a function of the layer thickness  $n$ .

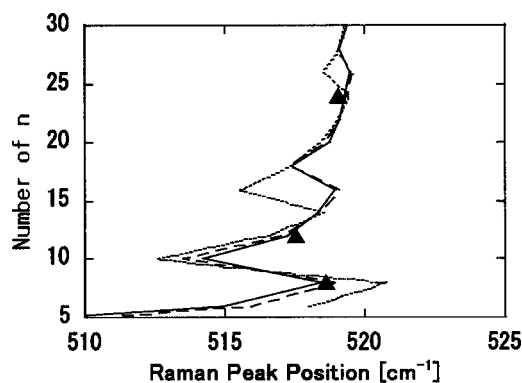


FIG. 5. Comparison of the experimentally observed  $LO_1(^{30}\text{Si})$  peak positions ( $\blacktriangle$ ) with calculations assuming intermixing of zero (solid curve), one (broken curve), and two (dotted curve) monolayers at the  $^{28}\text{Si}$  and  $^{30}\text{Si}$  interfaces.

except for the one detail: while  $LO_1(^{28}\text{Si})$  peaks in  $n=12$  and 24 samples are hidden in the large substrate peak, the  $LO_1(^{28}\text{Si})$  peak is observed experimentally for the  $n=8$  sample and its position deviates from the calculation. We suspect that the fluctuation in the periodicity revealed in Fig. 2 for the  $n=8$  sample is responsible for this deviation, because the peak position is very sensitive to any change in the layer thickness  $n$ . In turn it is possible to estimate the degree of interface mixing between  $^{28}\text{Si}$  and  $^{30}\text{Si}$  layers for our growth conditions by comparison with theory.<sup>26</sup> Figure 5 shows the comparison of the experimentally observed  $LO_1(^{30}\text{Si})$  peak positions with calculations assuming intermixing of zero, one, and two monolayers at the  $^{28}\text{Si}$  and  $^{30}\text{Si}$  interfaces.  $LO_1(^{30}\text{Si})$  is chosen because this is the only mode commonly observed in the three samples. We have inserted two and four layers of  $^{29}\text{Si}$ , which is the average mass of  $^{28}\text{Si}$  and  $^{30}\text{Si}$  when interdiffusion occurs, for the calculation of single and two layers of intermixing, respectively. The theoretical peak positions calculated assuming atomically abrupt  $^{28}\text{Si}/^{30}\text{Si}$  interfaces agree quantitatively with our experimental results, while those assuming intermixing fail to explain the observed peak positions. Therefore, interfaces of our isotopic Si superlattices are abrupt and the smearing of the profiles observed in Fig. 3 is a SIMS artifact.

In summary, we have successfully grown and characterized Si isotope superlattices. These samples will be available for a variety of basic studies probing isotope effects in low dimensional structures.

The authors would like to acknowledge K. Morita, J. Kato, T. Ohya, Y. Matsuki, and A. Fujimoto for fruitful dis-

cussions, and Professor K. Nakagawa for the development of the cells used in this study. The work has been supported in part by Silex Systems Ltd. (Australia) and by the Grants-in-Aid for Scientific Research for the Priority Areas Research (No. 14076215) by MEXT, Japan.

- <sup>1</sup>Y. Cui, X. Duan, J. Hu, and C. M. Lieber, *J. Phys. Chem. B* **104**, 5213 (2000).
- <sup>2</sup>B. E. Kane, *Nature (London)* **393**, 133 (1998).
- <sup>3</sup>T. D. Ladd, J. R. Goldman, F. Yamaguchi, Y. Yamamoto, E. Abe, and K. M. Itoh, *Phys. Rev. Lett.* **89**, 017901 (2002).
- <sup>4</sup>J. P. Gordon and K. D. Bowers, *Phys. Rev. Lett.* **1**, 368 (1958).
- <sup>5</sup>T. H. Geballe and G. W. Hull, *Phys. Rev.* **110**, 773 (1958).
- <sup>6</sup>D. K. Wilson, *Phys. Rev.* **134**, A265 (1964).
- <sup>7</sup>J. Spitzer, T. Ruf, M. Cardona, W. Dondl, R. Shorer, G. Abstreiter, and E. E. Haller, *Phys. Rev. Lett.* **72**, 1565 (1994).
- <sup>8</sup>K. Morita, K. M. Itoh, J. Muto, K. Mizoguchi, N. Usami, Y. Shiraki, and E. E. Haller, *Thin Solid Films* **369**, 405 (2000).
- <sup>9</sup>M. Nakajima, H. Harima, K. Morita, K. M. Itoh, K. Mizoguchi, and E. E. Haller, *Phys. Rev. B* **63**, 161304 (2001).
- <sup>10</sup>A. V. Kolobov, K. Morita, K. M. Itoh, and E. E. Haller, *Appl. Phys. Lett.* **81**, 3855 (2002).
- <sup>11</sup>E. E. Haller, *J. Appl. Phys.* **77**, 2857 (1995).
- <sup>12</sup>D. Karaiskaj, M. L. W. Thewalt, T. Ruf, M. Cardona, H.-J. Pohl, G. G. Devyatych, P. G. Sennikov, and H. Riemann, *Phys. Rev. Lett.* **86**, 6010 (2001).
- <sup>13</sup>D. Karaiskaj, M. L. W. Thewalt, T. Ruf, M. Cardona, and M. Konuma, *Phys. Rev. Lett.* **90**, 016404 (2003).
- <sup>14</sup>D. Karaiskaj, M. L. W. Thewalt, T. Ruf, M. Cardona, and M. Konuma, *Phys. Rev. Lett.* **89**, 016401 (2002).
- <sup>15</sup>J. Kato, K. M. Itoh, H. Yamada-Kaneta, and H.-J. Pohl, *Phys. Rev. B* **68**, 035205 (2003).
- <sup>16</sup>K. Takyu, K. M. Itoh, K. Oka, N. Saito, and V. I. Ozhogin, *Jpn. J. Appl. Phys., Part 1* **38**, L1493 (1999).
- <sup>17</sup>A. D. Bulanov, G. G. Devyatych, A. V. Gusev, P. G. Sennikov, H.-J. Pohl, H. Riemann, H. Schilling, and P. Becker, *Cryst. Res. Technol.* **35**, 1023 (2000).
- <sup>18</sup>P. Becker, H. Bettin, P. De Bievre, C. Holm, U. Kutgens, F. Spieweck, J. Stumpel, S. Valkiers, and W. Zulehner, *IEEE Trans. Instrum. Meas.* **44**, 522 (1995).
- <sup>19</sup>K. M. Itoh *et al.*, *Jpn. J. Appl. Phys.* (in press).
- <sup>20</sup>H. Bracht, E. E. Haller, and R. Clark-Phelps, *Phys. Rev. Lett.* **81**, 393 (1998).
- <sup>21</sup>A. Ural, P. B. Griffin, and J. D. Plummer, *Phys. Rev. Lett.* **83**, 3454 (1998).
- <sup>22</sup>T. Takahashi, S. Fukatsu, K. M. Itoh, M. Uematsu, A. Fujiwara, H. Kageshima, Y. Takahashi, and K. Shiraishi, *J. Appl. Phys.* **93**, 3674 (2003).
- <sup>23</sup>P. Molinàs-Mata and M. Cardona, *Phys. Rev. B* **43**, 9799 (1991).
- <sup>24</sup>H. D. Fuchs, P. Molinàs-Mata, and M. Cardona, *Superlattices Microstruct.* **13**, 447 (1993).
- <sup>25</sup>F. Widulle, T. Ruf, M. Konuma, I. Silier, M. Cardona, W. Kriegseis, and V. I. Ozhogin, *Solid State Commun.* **118**, 1 (2001).
- <sup>26</sup>E. Silveira, W. Dondl, G. Abstreiter, and E. E. Haller, *Phys. Rev. B* **56**, 2062 (1997).